Nitrogen Radio Frequency Plasma Processing of Fullerenes

Masafumi Ata,*,† Houjin Huang,† and Takeshi Akasaka‡

Material Laboratories, Sony Corporation, 2-1-1 Shinsakuragaoka, Hodogaya-ku, Yokohama, Kanagawa 240-0036, Japan, and Center for Tsukuba Advanced Research Alliance, Department of Chemistry, University of Tsukuba, Tsukuba, Ibaraki 305-8577, Japan

Received: July 10, 2003; In Final Form: February 1, 2004

Nitrogen radio frequency (rf) plasma processing of C_{60} in the formation of the nitrogen endohedral complex ($N@C_{60}$) and $C_{60}N$ adducts was fully examined with spectroscopic methodology and molecular orbital calculations. $N@C_{60}$ formation was achieved using an internal parallel plate electrode type of capacitively coupled nitrogen rf plasma,[1] whereas this was impossible when using an external ring electrode type of capacitively coupled rf nitrogen plasma. This experimental observation suggests that the formation of $N@C_{60}$ in the internal parallel plate plasma system stems from the steep charge gradient around the rf cathode electrode induced by the self-bias effect, which promotes accelerated collisions of N^+ with C_{60}. Another important nitrogen rf plasma-induced process is the formation of $C_{60}N$ adducts. The formation and relative stabilities of internal and external $C_{60}N$ adducts and $N@C_{60}$ were fully examined with the aid of MO calculations at a semiempirical approximation level, and the calculation was further extended to the plasma processing of C_{70}. The calculation suggested that a C_{60} polymer is abundantly formed in a nitrogen rf plasma in which the nitrogen plays an important role in the intermolecular cross-linking of C_{60}, derived from the radical addition and/or recombination reaction of the $C_{60}N$ adduct. The polymer formation was clearly supported by the observation of the peaks attributable to the nitrogen-containing C_{60} dimers in the time-of-flight mass spectra observed on the carbonaceous deposits formed in the nitrogen rf plasma.

Introduction

Following the first attempts at the production and extraction of a lanthanum endohedral C_{82} cage ($La@C_{82}$)[2] and its observation by ESR,[3] encapsulation of various elements within the fullerene cage has attracted great interest because of the resulting unique physical and chemical properties. Encapsulation of the group V element nitrogen in a C_{60} cage (i.e., $N@C_{60}$) was first achieved by Weidinger et al. using an ion implantation technique.[4] They also produced and extracted C_{60}, encapsulating molecular nitrogen, $N_2@C_{60}$, in the same manner.[5] Encapsulation of another group V element, phosphorus, in a C_{60} cage was also extensively investigated using the same technique.[6] A notable aspect which has been confirmed for group V elements encapsulated in C_{60} is that the nitrogen and phosphorus atoms locate at the center of the cage,[7−9] as has been theoretically supported by Greer.[10] In these endohedral molecules, charge separation between the trapped element and the C_{60} cage hardly occurs and the element retains an atomic nature in the cage. Thus, noncovalent atomic nitrogen encapsulated in a C_{60} cage presents a quartet electronic spin multiplicity which couples further with the ^{14}N nucleus, having nuclear spin quantum number $I = 1$ via Fermi contact. The atomic spin encapsulated in a C_{60} cage is free from direct interspin collision, which seriously affects the spin dipolar relaxation process. In practice, the ESR line width is very sharp, owing to its long spin−spin dipolar relaxation time. Dinse et al. observed a spin−lattice relaxation time of several hundred microseconds for $N@C_{60}$ using a pulse ESR system.[8] As a possible electronic structure for $N@C_{60}$, Lu et al. suggested that the 2p spin−orbital of atomic nitrogen locates in the HOMO−LUMO gap of the host C_{60}.[11]

In atomic nitrogen encapsulation, when forming $N@C_{60}$ by ion implantation, the kinetic energy of collision between the accelerated nitrogen cation from the ion source and the molecular fullerene evaporated from the effusion cell must be a key parameter for the yield of the endohedral complex. We anticipated that the rf nitrogen plasma would present a possible technique for the high yield formation of $N@C_{60}$, since the nitrogen cation is easily generated in the plasma, as is the introduction of C_{60} into the plasma using a heating probe. Advantages of the method are easy operation and adjustability of the process parameters, as mentioned in the literature.[1]

In the present paper, we examine the applicability of both the internal parallel plate type and the external ring electrode type of the capacitively coupled rf nitrogen plasma system for the nitrogen endohedral complex formation with C_{60}. Referring to the experimental findings, the kinetic processes in the formation of $N@C_{60}$ in the rf nitrogen plasma can be fully described by employing molecular orbital calculations at a semiempirical level. The approach is used in detail on the nitrogen plasma processing of C_{70} and on the prediction of the minimum size of a fullerene cage possible for the formation of a nitrogen endohedral complex. The interaction energy of atomic nitrogen with fullerene cages is discussed on the basis of the formation kinetics of $N@C_{60}$ and $N@C_{70}$. The calculation is used to clarify the relaxation process of the $C_{60}N$ open-shell adduct and predict the polymerization of the $C_{60}N$ adducts. To confirm the nitrogen-containing C_{60} polymer formation, time-of-flight mass spectrometry (TOF-MS) is performed on the C_{60} deposits formed on a substrate. Finally, the kinetic process of

* Present address: AIST Tsukuba.
† Sony Corporation.
‡ University of Tsukuba.

10.1021/jp035985w CCC: $27.50
Published on Web 03/20/2004

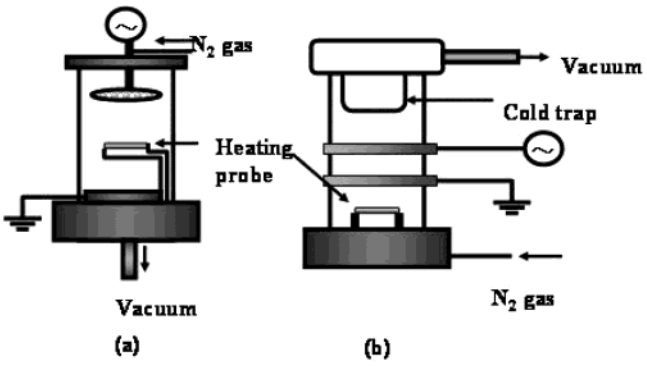

Figure 1. Schematic drawing of the internal parallel plate electrode type of the capacitively coupled rf plasma system (a) and the external ring electrode type of the capacitively coupled rf plasma system, equipped with two ring electrodes on the outer wall of the quartz-reactor (b).

C_{60} polymerization in a nitrogen rf plasma is characterized, comparing it with the C_{60} polymerization in an inert gas plasma, such as Ar, and identifying the difference in polymer cross-link structures.

Experimental Section

Two types of capacitively coupled rf plasma systems, as shown in Figure 1, were used for the rf plasma processing of fullerenes. The first was an internal parallel plate electrode type of the capacitively coupled rf plasma system, previously used for fullerene polymer generation in an Ar plasma.[12] The rf cathode electrode was 12 cm in diameter and was mounted in a glass bell jar reactor. The other equipment, built in-house, is of the external ring electrode type of the capacitively coupled rf plasma system, equipped with two ring electrodes on the outer wall of the quartz-reactor, as shown in Figure 1b. The outer electrode is not coil-shaped, so the system is not an inductively coupled plasma but is capacitively coupled. In both systems, a rf plasma at 13.56 MHz was generated in the glass reactor containing 99.999% pure nitrogen gas at 25 Pa. Samples of C_{60} were evaporated using a heated molybdenum probe.

After the exposure of C_{60} to the plasma, sample deposits were collected separately from the inner wall of the reactor, the electrode, and the Si substrate on the grounded electrode. The collected samples were dispersed in CS_2 and filtrated with a membrane filter. The filtrates were transferred into a glass apparatus and fully deoxygenated for ESR observation (JEOL, JES-RE2X). The third and fourth ESR peaks of the digital MnO_2 marker (JEOL) were used for estimation of the spin number. The TOF-MS spectra were observed to confirm the formation of the C_{60} nitrogen adduct and a C_{60} polymer derived from the C_{60} nitrogen adduct. A reflection type TOF-MS spectrometer from Shimadzu was used, equipped with a N_2 laser (337 nm) for ablation and ionization of the sample. Observation was performed without the use of any matrix molecule. Laser power was limited to a 100 μJ/pulse level to avoid the photoinduced polymerization of C_{60}. The diameter of the laser spot was 100 μm, and the pulse width was 3 ns.

Calculations

Semiempirical MNDO/AM-1[13] and PM-3 parametrizations[14] were adopted to examine possible kinetic processes of C_{60} in the nitrogen rf plasma. A software package, CAChe, based on MOPAC 2002 from Fujitsu Ltd. was used. For the calculation of nitrogen endohedral complexes, both doublet and quartet spin multiplicities were specified for comparison. The nitrogen external and internal adducts of C_{60} were examined on both the (5,6) and the (6,6) fusion bonds of the C_{60} molecule, and doublet spin multiplicities were specified for all of the nitrogen monoadducts of C_{60}. In the case of C_{70}, nitrogen adduct formation was examined for both the internal and the external adducts on the eight different types of C−C bonds.

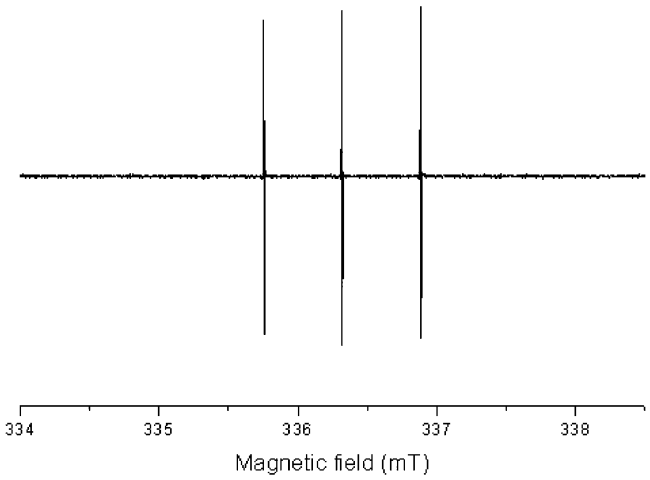

Figure 2. ESR spectrum of the CS_2 solution of N@C_{60} observed under deoxygenated conditions at ambient temperature.

Evaluation of the heats of reaction in the formation of the nitrogen adducts and nitrogen endohedral complexes of C_{60} was performed considering two possible mechanisms, that is, an ionic process ($C_{60} + N^+(T) + e$) and a radical process ($C_{60} + N^{\bullet}$-(Q)), where (T) and (Q) are abbreviations for triplet and quartet spin multiplicities, respectively. In the formation of the nitrogen-containing C_{60} polymer, a radical recombination reaction between two $C_{60}N$ adducts and a radical addition reaction between a $C_{60}N$ adduct and C_{60} were taken into account. The unrestricted Hartree−Fock method was adopted for all of the open-shell models. Thus, the heat of reaction so evaluated includes the energy difference owing to the different spin multiplicities of the chemical species before and after the reaction. Details of the calculation on fullerene materials have been described elsewhere.[15−18]

Results and Discussions

Experimental Results of RF Nitrogen Plasma. First, we performed nitrogen rf plasma processing of C_{60} at a plasma power of 30 W, aiming for the generation of N@C_{60}. After plasma operation, the carbonaceous deposits were collected from the sidewall of the reactor and dipped into CS_2. The filtrated CS_2 solution was slightly brownish purple. Figure 2 shows the ESR spectrum of the CS_2 solution after degas operation. This ESR active species is attributable to N@C_{60}.[1] The yield of N@C_{60} was evaluated from the integrated intensity ratio of the ESR signal of N@C_{60} and compared to that of the weighted, stable DPPH radical by reference to the digital MnO_2 marker. In the evaluation, microwave power is suppressed to 0.1 mW to avoid power saturation. The yield of N@C_{60} so evaluated was 0.02−0.05%.

One notable advantage in the plasma process is that the electronic excitation of the plasma gas is independent of the symmetry of the gas molecule, enhancing the efficiency of excitation. In our system, being of a nonequilibrium rf plasma type, only the electrons are activated to a high temperature. In the initial stage of the generation of atomic N and N^+ species in the nitrogen plasma, the ground state of molecular nitrogen is efficiently elevated by collision with highly energetic electrons

to electronically excited states. This electronic excitation process does not follow the symmetry rule of the photoexcitation process. Direct electronic excitation of the ground $X^1\Sigma_g^+$ state of molecular nitrogen to the triplet excited $A^3\Pi_u$ state is precipitated by the activated electron, irrespective of the process being a transition between orthogonal spin functional states.[19] The nitrogen molecule in the triplet excited $A^3\Pi_u$ state is metastable, since there is no effective spin−orbit process to the ground state in the molecular system. In the $A^3\Pi_u$ state, the electron configuration effectively induces inter-nitrogen nuclear repulsion. Further electronic excitation of the $A^3\Pi_u$ state appears to result in the generation of atomic nitrogen and/or its cation species, either directly or stepwise, as

$$N_2(X^1\Sigma_g) + e^* \rightarrow N_2^*(A^3\Pi_u) + e$$

$$N_2^*(A^3\Pi_u) + e^* \rightarrow N + N^+ + 2e$$

where * indicates the excited state and/or high temperature.

As mentioned in the literature, we could obtain $N@C_{60}$ under a moderately limited plasma power condition using the internal capacitively coupled plasma mode.[1] The plasma power applied is adequate for plasma polymerization of organic materials and fullerenes in an inert gas atmosphere, such as Ar.[12] As mentioned above, $N@C_{60}$ was extracted only from the deposit on the sidewall of the bell-jar-shaped reactor and the Si substrate on the ground electrode. Deposition of the carbonaceous material on the surface of the upper cathode electrode was also observed during the course of the plasma operation. Neither $N@C_{60}$ nor an intact cage of C_{60} was extracted with CS_2 from the carbonaceous deposit on the cathode electrode. The Raman observation of the carbonaceous deposit suggested that the microscopic structure of the material is amorphous, such as carbon, indicating that C_{60} was seriously damaged by bombardment with N^+ and/or by a sputtering effect on the electrode

To avoid such serious damage of C_{60} on the cathode electrode, we made an external ring electrode type of the capacitively coupled rf nitrogen plasma system, as shown in Figure 1b. The formation of $N@C_{60}$ was examined in the plasma power range 10−300 W in this case. In this outer ring electrode geometry, the plasma gas forms a positive column, since the generation of N^+ is naturally effective, and the potential falls to zero at the grounded anode electrode.[20,21] In contrast to the successful generation of $N@C_{60}$ with the internal capacitively coupled system, the endohedral complex was not generated with the external ring system under any condition. Thus, the introduction of the cathode electrode inside the reactor seems to be crucial and essential for $N@C_{60}$ generation.

In the internal cathode geometry, the cathode electrode is negatively charged by the self-bias effect at 250−300 V and the plasma potential is positive. A potential difference of some hundreds of volts across the cathode sheath accelerates ionized species such as N^+ toward the cathode electrode. A key process for $N@C_{60}$ formation must be the collision between accelerated N^+ and C_{60} in the peripheral region of the cathode electrode in the rf nitrogen plasma. In the case of the outer ring electrode geometry, however, N^+ is unable to acquire sufficient kinetic energy for $N@C_{60}$ formation, as the plasma gas is positively charged throughout the reactor. Thus, the incorporation of atomic nitrogen in a C_{60} cage using an internal parallel plate electrode type of capacitively coupled rf nitrogen plasma could be regarded as a plasma-based ion implantation process which occurs selectively at the sheath area of the cathode electrode. In practice, the yield of $N@C_{60}$ was increased up to 0.05% when the C_{60} sample was evaporated from a Mo boat located close to the cathode electrode, enabling the effective supply of C_{60} to the sheath area of the cathode electrode, where the potential difference induced the acceleration of N^+.

TABLE 1: Heats of Formation of the $C_{60}N$ Adducts and $N@C_{60}$

	$\Delta H_f°$ (kcal/mol)			
	AM-1		PM-3	
compound[a]	outer	inner	outer	inner
(6,6)-$C_{60}N$ adduct	1001.2	1127.0	843.5	944.9
(5,6)-$C_{60}N$ adduct	990.2	1146.0	827.9	955.4
$N@C_{60}$ (doublet)		1107.1		943.9
$N@C_{60}$ (quartet)		1075.0		921.1

[a] The doublet spin multiplicities were specified for all of the internal and external $C_{60}N$ adducts. The $\Delta H_f°$ values for the C_{60} molecule were 927.7 and 811.0 kcal/mol at the AM-1 and PM-3 parametrizations, respectively.

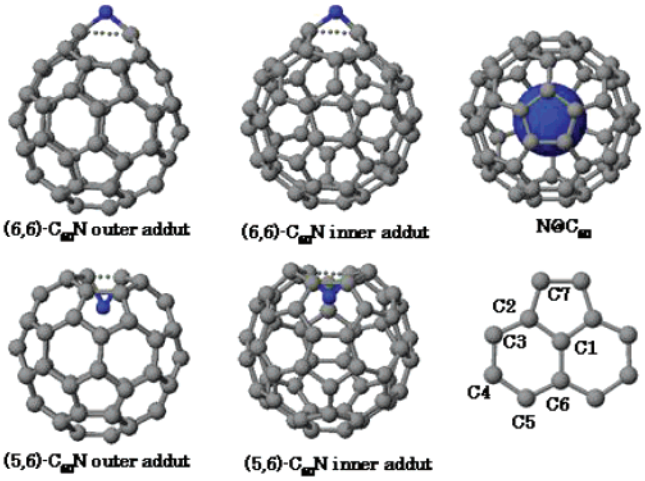

Figure 3. Molecular structures of the external and internal $C_{60}N$ adducts and $N@C_{60}$ optimized at the MNDO/AM-1 level. The inset shows the partial structure of C_{60} and the numbering system used in this work.

Another yield-controlling factor is the purity of the plasma gas. Namely, the nitrogen encapsulation process in the internal parallel plate system was highly sensitive to the purity of the nitrogen gas. Trace amounts of oxygen appear to markedly affect the generation and/or life of N^+ in the rf plasma. Otherwise, highly active excited singlet O_2 generated in rf plasma may work as a scavenger of $N@C_{60}$.

Nitrogen Plasma Processing of C_{60}. In this section, nitrogen rf plasma processing of C_{60} is examined with reference to molecular orbital calculations. As mentioned above, N and N^+ are abundant chemical species generated in nitrogen rf plasma. Radical addition of N to C_{60} and implantation of N^+ into C_{60} may form $C_{60}N$ adducts and $N@C_{60}$, respectively. The values of heat of formation ($\Delta H_f°$) for the open-shell $C_{60}N$ adducts and $N@C_{60}$ are presented in Table 1, and the corresponding molecular structures are shown in Figure 3. The C_1-C_6 and C_1-C_2 bonds shown in the inset of Figure 3 are noted as (6,6) and (5,6) fusion bonds, respectively. Although both the (6,6)-$C_{60}N$ outer adduct and the (5,6)-$C_{60}N$ outer adduct have local minimum structures, the structures shown in Figure 3 are more stable ones.

All other nitrogen outer cage adducts having an −N− bridge on two non-neighboring carbons such as C_1-N-C_3, C_1-N-C_4, C_1-N-C_5, and C_1-N-C_7 were first optimized using a molecular mechanics (MM) procedure, and then the structures

TABLE 2: Heats of Reaction in the Formation of the C_{60} Nitrogen Adducts and N@C_{60}

	AM-1		PM-3	
compound[a]	$\Delta H_f°$(r)/ion[b] (kcal/mol)	ΔH_f(r)/rad[c] (kcal/mol)	$\Delta H_f°$(r)/ion[b] (kcal/mol)	ΔH_f(r)/rad[c] (kcal/mol)
(6,6)-C_{60}N outer adduct	−388.8	−84.5	−386.8	−80.5
(5,6)-C_{60}N outer adduct	−398.8	−95.5	−402.4	−96.1
(6,6)-C_{60}N inner adduct	−260.3	+41.3	−285.4	+20.9
(5,6)-C_{60}N inner adduct	−244.0	+60.3	−274.9	+31.4
N@C_{60}	−315.0	−10.7	−309.2	−2.9

[a] The doublet and quartet spin multiplicities were specified for all of the C_{60}N adducts and the endohedral complex, respectively. [b] The heats of reaction of the nitrogen adducts and the endohedral complex via collision of C_{60} with N^+ having triplet spin multiplicity. [c] The heats of reaction of those compounds via the radical addition reaction of atomic nitrogen to a C_{60} molecule.

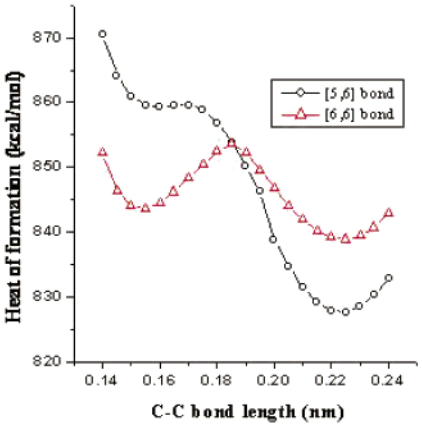

Figure 4. Correlation between the MNDO/PM-3 heats of formation of the (5,6)- and (6,6)-C_{60}N outer adducts and their C−C bond lengths.

were used for the MO calculation. Further MO optimization of these structures indicated that the C_{60} nitrogen adducts on C_1−N−C_3, C_1−N−C_4, and C_1−N−C_5 were spontaneously transformed to the C_1−N−C_6 form, whereas the C_1−N−C_7 adducts were transformed to the C_1−N−C_2 form. Thus, the nitrogen adducts shown in Figure 3 appear to be possible forms of the C_{60}N adduct which could be created in a nitrogen rf plasma.

A notable aspect in Table 1 is the fact that nitrogen addition to the (5,6) fusion bond is slightly more stable than that to the (6,6) fusion bond in contrast to the case of the usual addition reaction to a C_{60} cage. The increased stability of (5,6)-C_{60}N compared to (6,6)-C_{60}N is argued in analogy with the case of C_{60} mono-oxide. A stable form of C_{60} oxide, (5,6) open C_{60}O, was synthesized by the photochemical method and fully characterized by Weisman et al.[22] and Escobedo et al.[23] Kepert et al. suggested that the oxidation of the (5,6) fusion bond results in bond breaking.[24] Thus, C−C bond length-dependent structural stability was examined for the C_{60} outer nitrogen adducts. Figure 4 shows the (5,6) and (6,6) C−C bond length-dependent $\Delta H_f°$ values of (6,6)- and (5,6)-C_{60}N obtained at the PM-3 level. Local minimum points exist for both the (6,6)-C_{60}N and (5,6)-C_{60}N adducts. In both adducts, (6,6) and (5,6) open structures were more stable than (6,6) and (5,6) closed structures. Thus, the C−C bond opening of the (5,6) fusion bond results in the stabilization of the (5,6)-C_{60}N adducts.

In the case of N@C_{60}, the quartet spin multiplicity was predicted to be more stable than the doublet multiplicity, indicating that the nitrogen atom is still atomic in nature. The main energy difference between the doublet and quartet spin multiplicities is attributable to the increased level of the spin exchange contribution. These results are consistent with the theoretical prediction by Mauser et al.[25] Although the spin multiplicities are different for the N@C_{60} and C_{60}N adducts, N@C_{60} is predicted to be less stable than the outer C_{60}N adducts and more stable than the inner C_{60}N adducts.

The values of the heat of reaction (ΔH_f(r)) in the formation of the C_{60}N adducts and N@C_{60} are presented in Table 2. In this table, ΔH_f(r)/ion is the value for the formation of materials by the collision of N^+ and C_{60}, whereas ΔH_f(r)/rad refers to that for the radical addition reaction between atomic nitrogen and C_{60}:

$$N^+(T) + C_{60} + e \rightarrow C_{60}N(D) \quad \text{or} \quad N@C_{60}(Q)$$

$$N^{\bullet}(Q) + C_{60} \rightarrow C_{60}N(D) \quad \text{or} \quad N@C_{60}(Q)$$

Although we must give consideration to the differences in spin multiplicities of the chemical species participating in the reaction, all of the ionic processes in the formation of the C_{60}N adducts and N@C_{60} are predicted to be largely exothermic. The reason is that the $\Delta H_f°$ values for atomic N having a quartet spin multiplicity and N^+ having a triplet spin multiplicity are fixed to be 113.0 and 417.3 kcal/mol, respectively, at both the AM-1 and PM-3 parametrizations. Thus, ΔH_f(r)/rad differs from ΔH_f(r)/ion by ∼300 kcal/mol for each model.

Taking into account the above results and discussion, evaluation of the exact heats of reaction in the formation of the C_{60}N adducts and N@C_{60} is somewhat uncertain. In the case of the formation of N@C_{60}, participation of the ion species N^+ is strongly suggested from experiment. Nevertheless, the ΔH_f(r)/rad seems to be a possible measure of the probability of the generation of N@C_{60}. The data also indicate the relative stabilities of the C_{60}N adducts and N@C_{60}. The outer C_{60}N adduct appears to be generated abundantly in the nitrogen plasma, while the inner C_{60}N adduct is hardly formed, owing to its highly strained valence structure. The remarkable aspect of the process is that the quartet N@C_{60} is predicted to be more stable than the nitrogen inner adducts.

As shown in Table 2, the ΔH_f(r)/rad in the formation of N@C_{60} from atomic nitrogen and C_{60} is predicted to be −10.7 and −2.9 kcal/mol with the AM-1 and PM-3 parametrizations, respectively. This value is consistent with the interaction energy of atomic nitrogen with the C_{60} cage, which was predicted to be −7.34 kcal/mol for N@C_{60} at the 6-31G* basis set level.[26] BelBruno[27] reported that the ΔH_f(r) for N@C_{60} is predicted to be exothermic by 0.082 eV; however, the density functional theory method predicted it to be slightly endothermic. These results support the fact that the interaction between nitrogen and the C_{60} cage is not particularly large; hence, the nitrogen maintains its atomic nature in the C_{60} cage.

As pointed out in the literature regarding N@C_{60}, this calculation suggested that the nitrogen locates at the center of the C_{60} cage. This is closely related to the adsorption phenomenon in carbon nanotubes, which was investigated by Dillon et al.[28] Kaneko et al.[29,30] have extensively examined the adsorption mechanism in terms of supercritical hydrogen in a nanospace formed within single walled carbon nanotubes. We have reported

TABLE 3: Heats of Formation of the $C_{70}N$ Adducts and $N@C_{70}$

	$\Delta H_f°$ (kcal/mol)			
	AM-1		PM-3	
compound[a]	outer	inner	outer	inner
$C_{70}N$ ①-adduct	1069.1	1213.4	881.4	1009.3
$C_{70}N$ ②-adduct	1082.8	1213.4	892.4	1009.3
$C_{70}N$ ③-adduct	1055.4	1213.4	880.0	1009.3
$C_{70}N$ ④-adduct	1072.2	1190.4	896.4	1010.5
$C_{70}N$ ⑤-adduct	1061.4	1209.6	885.6	988.7
$C_{70}N$ ⑥-adduct	1060.1	1192.5	884.7	999.7
$C_{70}N$ ⑦-adduct	1073.5	1178.0	896.7	985.7
$C_{70}N$ ⑧-adduct	1057.1	1191.5	887.8	1005.8
$N@C_{70}$ (doublet)	1169.8		991.6	
$N@C_{70}$ (quartet)	1137.7		969.7	

[a] The $\Delta H_f°$ values for the C_{70} molecule were 1061.2 and 883.4 kcal/mol at the AM-1 and PM-3 parametrizations, respectively. The doublet spin multiplicities were specified for all of the $C_{70}N$ adducts.

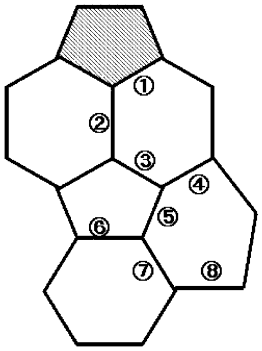

Figure 5. Bond notation system used for the C_{70} molecule. The molecular axis is passed through the center of the top pentagon. Bond ⑧ is the equatorial bond of the C_{70} molecule.

the importance of subnanospaces for hydrogen adsorption.[31,32] The cavity in a C_{60} cage is a finite subnanosized space, and the optimized structure of $N@C_{60}$ indicates that the nitrogen atom interacts more strongly with the subnanospace than with the inner wall of the C_{60}.

Nitrogen Plasma Processing of C_{70}. The $\Delta H_f°$ values for the outer and inner $C_{70}N$ adducts and $N@C_{70}$ are presented in Table 3, and the corresponding numbering for C_{70} is shown in Figure 5. For the intermolecular [2 + 2]-cycloaddition reaction between C_{70} molecules, bonds 2 and 8 were predicted to be the most and least active, respectively.[17] In contrast to the ease of the cycloaddition reaction, it was speculated that outer $C_{60}N$ adduct formation would occur preferentially on bond 8 but rarely would occur on bond 2. Also, the outer $C_{70}N$ adduct on bond 2 is less stable than that on bonds 1 and 3, indicating outer $C_{70}N$ adduct formation occurs preferentially on the (5,6) fusion bonds. This result is consistent with the fact that the outer $C_{60}N$ adduct is formed on a (5,6) fusion bond, as mentioned above. Concerning inner $C_{70}N$ adducts, those formed on bonds 1 and 2 were spontaneously transformed to the inner adduct on bond 3 in both the AM-1 and PM-3 parametrizations. This result suggests that nitrogen migration occurs within the cage even after inner adduct formation.

The $\Delta H_f(r)$ values in the formation of $N@C_{70}$ via the radical addition reaction of N to C_{70} were evaluated to be −36.5 and −26.7 kcal/mol with the AM-1 and PM-3 parametrizations, respectively. As mentioned above, these values are regarded as the energies of interaction between N and the C_{70} cage, indicating that the interaction energy is increased in $N@C_{70}$ over that in $N@C_{60}$. This increased level of interaction energy in $N@C_{70}$ is attributable to the increased π-conjugation in C_{70} over that in C_{60}. The dominant part of the interaction energy is the dispersion force of the atomic nitrogen and the inside of the fullerene cage, so the physisorption energy could be increased with increased π-conjugation in C_{70} compared to C_{60}. This variation in the level of interaction with π-conjugation is well supported by the fact that the polarizability of C_{70} is increased with respect to that of C_{60}[33,34] and closely related to the fact that the g-value in the electron spin resonance spectrum of $N@C_{70}$ is slightly shifted from that of $N@C_{60}$.[4b]

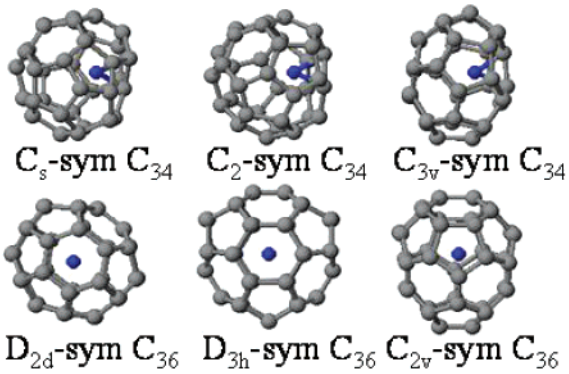

Figure 6. MNDO/AM-1 optimized structures of molecular mechanics optimized $N@C_{34}$ and $N@C_{36}$. Molecular mechanics optimized $N@C_{34}$ structures, having C_s, C_2, and C_{3v} symmetry, were spontaneously transformed to the internal $C_{60}N$ adducts during the course of structure optimization iteration, while C_{36} cages, having D_{2d}, D_{3h}, and C_{2v} symmetry, were optimized to $N@C_{36}$ structures.

Minimum Size of Nitrogen Endohedral Fullerene. Here, we briefly discuss the minimum cage size of fullerene possible for the formation of $N@C_n$ using MO calculations. Figure 6 shows the optimized structures of $N@C_{34}$ and $N@C_{36}$. These structures were optimized first by MM and finally by MO at the MNDO/AM-1 level. As can be seen, the nitrogen atom forms a valence bond with C_s-, C_2-, and C_{3v}-symmetry C_{34} cages, while a nitrogen endohedral complex is possible for D_{2d}-, D_{3h}-, and C_{2v}-symmetry C_{36} cages. Thus, the minimum cage size possible to form the nitrogen endohedral complex would appear to be C_{36}. In these $N@C_{36}$ structures, the cavity diameter is in the range 0.53−0.60 nm.

The interaction energies of $N@C_{36}$, which were evaluated as $\Delta H_f(r)$/rad in the above section, were evaluated for D_{2d}-, D_{3h}-, and C_{2v}-symmetry $N@C_{36}$ to be −7.7, −11.5, and −3.4 kcal/mol at the AM-1 level and −12.5, −3.7, and −7.2 kcal/mol at the PM-3 level, respectively. These stabilization levels are identical to those for $N@C_{60}$.

N-Participated C_{60} Polymer Formation. As we have described in the literature,[1] the probability of $N@C_{60}$ formation with the capacitively coupled rf plasma mode is fairly low. The above calculated result of the rf nitrogen plasma process of C_{60} suggested that nitrogen addition on the C_{60} cage is the major process. This $C_{60}N$ adduct is still an open-shell condition at the nitrogen, suggesting the material is still active toward the addition reaction. In the case where the $C_{60}N$ adduct reacts with C_{60}, $(C_{60})_2N$ is predicted to be a possible stable dimer structure, whereas the addition reaction between two $C_{60}N$ adducts results in the formation of $(C_{60}N)_2$. Figure 7 shows all of the possible C_{60} dimer species derived from the $C_{60}N$ adduct, in which nitrogen takes part in the intermolecular linking. The $\Delta H_f°$ values for the inner structures and their $\Delta H_f(r)$ values for the radical addition reaction are presented in Table 4. From the ΔH_f-(r), the formation of both (6,6)-$C_{120}N$ and (5,6)-$C_{120}N$ is predicted to be an exothermic process. A notable aspect is that the $C_{60}N$ outer (5,6) adduct was more stable than the $C_{60}N$ outer

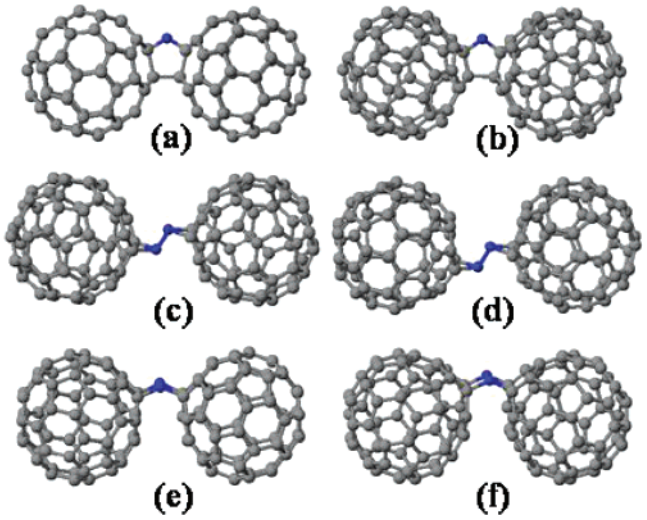

Figure 7. Optimized molecular structures of $C_{120}N$ and $C_{120}N_2$ at the MNDO/AM-1 level. Structures a and b are generated by the radical addition reaction of $C_{60}N$ to C_{60}, and structures c−f are formed by the radical recombination reaction between two $C_{60}N$ adducts.

TABLE 4: Heats of Formation of the Nitrogen-Containing C_{60} Dimers and Heats of Reaction in the Formation of Those Dimers

	AM-1		PM-3	
dimer[a]	$\Delta H_f°$ (kcal/mol)	ΔH_f(r)/new (kcal/mol)	$\Delta H_f°$ (kcal/mol)	ΔH_f(r)/new (kcal/mol)
(6,6)-$C_{120}N$ (a)	1905.4	−68.5	1578.5	−76.0
(5,6)-$C_{120}N$ (b)	1927.6	−41.6	1597.9	−41.0
(6,6)-$C_{120}N_2$ (c)	2009.8	+7.4	1671.9	−15.1
(5,6)-$C_{120}N_2$ (d)	2010.5	+17.5	1668.9	+13.1
(6,6)-$C_{120}N_2$ (e)	2019.4	+17.0	1647.9	−7.9
(5,6)-$C_{120}N_2$ (f)	2060.2	+67.2	1689.4	+33.6

[a] The corresponding nitrogen-containing C_{60} dimer structures shown in parentheses in this column were collected in Figure 7.

(6,6) adduct, whereas (6,6)-$C_{120}N$ was more stable than (5,6)-$C_{120}N$. The increased stability of (6,6)-$C_{120}N$ is attributable to the formation of an inter-C_{60} C−C pivot bond compatible with the (6,6) fusion bonding of C_{60}.

Among the $C_{120}N_2$ structures shown in Figure 7c−e, formation of (5,6)-$C_{120}N_2$ is predicted to be endothermic by 67.2 and 33.6 kcal/mol with the AM-1 and PM-3 parametrizations in Figure 7c and d, respectively, while the other $C_{120}N_2$ structure, shown in Figure 7e, appears to be impossible. Despite the singlet spin multiplicities of the $C_{120}N_2$ structures, these structures are not very stable, as can be seen in Table 4. The highly strained intermolecular =N−N= and −N=N− bonds could provide a possible reason for the poor stabilization of the $C_{120}N_2$ structures.

TOF-MS Observation. To confirm that the nitrogen participated in the polymerization of C_{60}, the deposits formed during the course of the rf nitrogen plasma processing were observed using TOF-MS. As we have mentioned in the literature,[16,17] laser power needs to be reduced to a level at which photoinduced polymerization of C_{60} is avoided when this method is adopted to identify intermolecular cross-linking. However, direct abrasion and ionization of the deposits was difficult, and fragment peaks were observed only at highly increased laser power. An intense peak was observed at $m/e = 26$ with an increased laser power. The peak is attributable to the fragment ion CN^- from the deposits, indicating that C−N bonding is formed in the deposits and the partial structure is fragile against the laser abrasion. It was difficult to discuss the partial structure of the deposits from the TOF-MS, since the mass profile strongly depended on the laser power. Thus, we tried to check the TOF-MS of the toluene-soluble chemical species extracted from the deposits by ultrasonication. Prior to the observation, the toluene solution was filtrated with a membrane filter and dried under vacuum conditions.

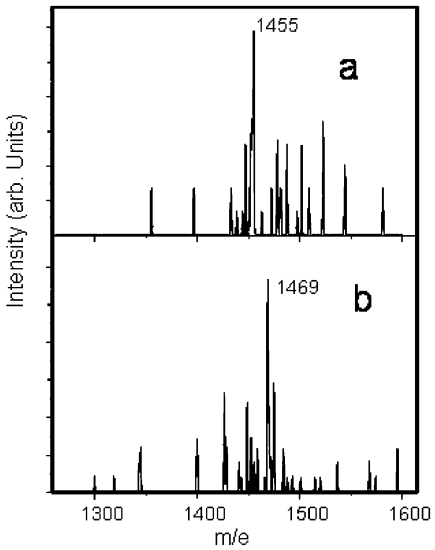

Figure 8. Reflectron type TOF-MS spectra of the toluene-extracted materials from the carbonaceous deposits formed on a Si substrate during the course of the nitrogen rf plasma process of C_{60}. Spectrums a and b were observed at laser powers of 105 and 114 μJ/pulse, respectively. These laser powers are slightly higher than the ablation threshold. Data were accumulated 50 times in both cases.

Figure 8a shows TOF-MS observations of the carbonaceous materials extracted from the deposits formed on the substrate during the nitrogen plasma processing of C_{60}. The observation was performed at a laser power slightly above the ablation threshold, with the data recorded 50 times for each observation. The most intense peak in the dimer region was observed at $m/e = 1455$. Taking into account the natural abundance of ^{13}C, this peak is attributable to the $C_{120}N^-$ ion. The spectrum shown in Figure 8b was observed with a slightly increased laser adsorption power than that of Figure 8a. In this case, the most intense peak was observed at $m/e = 1469$, indicating the ablated and ionized species $C_{120}N_2^-$. These results strongly suggest the formation of C_{60} dimers in which nitrogen participates in the intermolecular cross-linking, as shown in Figure 6. A notable aspect of the mass distribution profile in the dimer mass region is that the peaks attributable to the C_{60} dimer (i.e., C_{120}, C_{118}, and C_{116}), as observed in the deposit using an rf Ar plasma process,[16] were scarcely observed in this case. This observation strongly suggests the fact that nitrogen-participated polymerization of C_{60} is occurring in an rf nitrogen plasma in preference to the direct cross-linking of C_{60} molecules.

Goedde et al.[35] also reported on the dimer structure formed by ion implantation. This dimer is formed by the [2 + 2]-cycloaddition reaction between $N@C_{60}$ and C_{60}, that is, $N@C_{60}$=C_{60}. In our rf nitrogen plasma processing of C_{60}, the probability of $N@C_{60}$ formation is less than 0.1% of the amount of C_{60} introduced in the plasma. Thus, the intense peak observed in the TOF-MS shown in Figure 8 is not attributed to $N@C_{60}$=C_{60} but to C_{60}−N−C_{60}, as shown in Figure 7a and b.

The oxygen-bridged fullerene dimer $C_{120}O$ was recognized in 1995[36] and has been fully characterized.[37−39] The odd-numbered C_{60} dimer C_{121} was prepared and fully characterized.[40−42] The Aza-substituted fullerene $C_{59}N$ and its dimer are also well-known structures.[43−45] The intermolecular combina-

tion recognized in this study is different from these well-known structures, indicating a new class of intermolecular combinations derived from the $C_{60}N$ adducts.

Concluding Remarks

The possibility of the nitrogen rf plasma processing of C_{60} and C_{70} was fully examined experimentally and theoretically. The formation of $N@C_{60}$ in a nitrogen rf plasma was ascribed to the potential difference at the sheath area of the cathode, providing a self-bias effect, inducing acceleration of the ionized species N^+ toward the cathode electrode. In this case, the nitrogen encapsulation process could be regarded as a plasma-based ion implantation process. The increase in interaction energy between the encapsulated nitrogen and the cage in $N@C_{70}$ over that in $N@C_{60}$ results from the increased π-conjugation in C_{70}. The minimum size of fullerene possible to form a nitrogen endohedral complex was speculated to be C_{36}, having D_{2d}, D_{3h}, and C_{2v} symmetry.

A special aspect in nitrogen rf plasma is the abundant generation of not only the nitrogen cation but also atomic nitrogen. MO calculations suggested that the outer $C_{60}N$ adduct is formed abundantly by the radical addition reaction of atomic nitrogen to the C_{60} cage during the course of rf nitrogen plasma processing. Calculation also suggested that the radical recombination between the $C_{60}N$ adducts and the radical addition of $C_{60}N$ with C_{60} result in the formation of a new polymeric phase of C_{60}. The C_{60} dimer, in which nitrogen participates in the inter-C_{60} cross-linking, was clearly recognized in the dimer mass region of the TOF-MS spectra observed for the toluene-extracted materials from carbonaceous deposits formed during the course of the nitrogen rf plasma processing of C_{60}.

Acknowledgment. The authors thank Prof. Dr. T. Kato of the Institute of Molecular Science for fruitful discussions on the ESR detection of the endohedral complex and Mr. M. Miyakoshi and his colleagues of Sony Material Laboratories for professional drawing and machining of the in-house built plasma apparatus used in this work.

References and Notes

(1) Huang, H.; Ata, M.; Ramm, M. *Chem. Commun.* **2002**, 2076.
(2) Chai, Y.; Guo, T.; Jin, C.; Haufler, R. E.; Chibante, L. P. F.; Fure, J.; Wang, L.; Alford, J. M.; Smalley, R. E. *J. Phys. Chem.* **1991**, *95*, 7564.
(3) Johnson, R. D.; de Vries, M. S.; Salem, J.; Bethune, D. S.; Yannoni, C. S. *Nature* **1992**, *355*, 239.
(4) (a) Almeida Murphy, T.; Pawlik, Th.; Weidinger, A.; Hohne, M.; Alcala, R.; Spaeth, J.-M. *Phys. Rev. Lett.* **1996**, *77*, 1075. (b) Pietzak, B.; Waiblinger, M.; Almeida Murphy, T.; Weidinger, A.; Hörne, M.; Dietel, E.; Hirsch, A. *Carbon* **1998**, *36*, 613. (c) Weidinger, A.; Waiblinger, M.; Pietzak, B.; Almeida Murphy, T. *Appl. Phys. A* **1998**, *66*, 287. (d) Lips, K.; Waiblinger, M.; Pietzak, B.; Weidinger, A. *Phys. Status Solidi A* **2000**, *177*, 81.
(5) Suetsuna, T.; Doragoe, N.; Harniet, W.; Weidinger, A.; Shimotani, H.; Ito, S.; Takagi, H.; Kitazawa, K. *Chem.—Eur. J.* **2002**, *8*, 5080.
(6) (a) Knapp, C.; Weiden, N.; Käss, H.; Dinse, K.-P.; Pietzak, B.; Waiblinger, M.; Weidinger, A. *Mol. Phys.* **1998**, *95*, 999. (b) Larsson, J. A.; Gree, J. C.; Harniet, W.; Weidinger, A. *J. Chem. Phys.* **2002**, *116*, 7849.
(7) Knapp, C.; Weiden, N.; Käss, H.; Dinse, K.-P.; Pietzak, B.; Waiblinger, M.; Weidinger, A. *Mol. Phys.* **1998**, *95*, 999.
(8) (a) Knapp, C.; Dinse, K.-P.; Pietzak, B.; Waiblinger, M.; Weidinger, A. *Chem. Phys. Lett.* **1997**, *272*, 433. (b) Dietel, E.; Hirsch, A.; Pietzak, B.; Waiblinger, M.; Lips, K.; Weidinger, A.; Gross, A.; Dinse, P. *J. Am. Chem. Soc.* **1999**, *121*, 2432. (c) Dinse, K.-P.; Käss, H.; Knapp, C.; Weiden, N. *Carbon* **2000**, *38*, 1635.
(9) Weidinger, A.; Waiblinger, M.; Pietzak, B.; Almeida Murphy, A. *Appl. Phys. A: Mater. Sci. Process.* **1998**, *66*, 287.
(10) Greer, J. C. *Chem. Phys. Lett.* **2000**, *362*, 567.
(11) Lu, J.; Zhang, X.; Zhao, X. *Chem. Phys. Lett.* **1999**, *312*, 85.
(12) Takahashi, N.; Dock, H.; Matsuzawa, N.; Ata, M. *J. Appl. Phys.* **1993**, *74*, 5790.
(13) Dewar, M. J. S.; Zoebisch, E. G.; Healy, E. F.; Stewart, J. J. P. *J. Am. Chem. Soc.* **1985**, *107*, 3902.
(14) Stewart, J. J. P. *J. Comput. Chem.* **1989**, *10*, 209.
(15) Matsuzawa, N.; Ata, M.; Dixon, D. A.; Fitzgerald, G. *J. Phys. Chem.* **1994**, *98*, 2555.
(16) Ata, M.; Takahashi, N.; Nojima, K. *J. Phys. Chem.* **1994**, *98*, 9960.
(17) Ata, M.; Kurihara, K.; Takahashi, N. *J. Phys. Chem. B* **1997**, *101*, 5.
(18) Strasser, P.; Ata, M. *J. Phys. Chem. B* **1998**, *102*, 4131.
(19) (a) Baker, R. R.; Jacob, A.; Winkler, C. A. *Can. J. Chem.* **1970**, *49*, 1671. (b) Baker, R. R.; Jacob, A. *Can. J. Chem.* **1971**, *49*, 167. (c) Briner, E.; Kunig, J. J.; Tolun, R. *Helv. Chim. Acta* **1945**, *28*, 714.
(20) Hosokawa, N.; Tsukada, T.; Misumi, T. *J. Vac. Sci. Technol.* **1977**, *14*, 143.
(21) Vossen, J. L. *J. Electrochem. Soc.* **1979**, *126*, 319.
(22) Weisman, R. B.; Heyman, D.; Bachilo, S. M. *J. Am. Chem. Soc.* **2001**, *123*, 9720.
(23) Escobedo, J. O.; Frey, A. E.; Stronggin, R. M. *Tetrahedron Lett.* **2002**, *43*, 6117.
(24) Kepert, D. L.; Clare, B. W. *Inorg. Chim. Acta* **2002**, *327*, 41.
(25) Mauser, H.; van Eikema Hommes, N. J. R.; Clark, T.; Hirsch, A.; Pietzak, B.; Weidinger, A.; Dunsch, L. *Angew. Chem., Int. Ed. Engl.* **1997**, *36*, 2835.
(26) Park, J. M.; Tarakeshwar, P.; Kim, K. S.; Clark, T. *J. Chem. Phys.* **2002**, *116*, 10684.
(27) BelBruno, J. J. *Fullerenes, Nanotubes, Carbon Nanostruct.* **2002**, *10*, 23.
(28) Dillon, A. C.; Jones, K. M.; Bekkedahl, T. A.; Kiang, C. H.; Bethune, D. S.; Heben, M. J. *Nature* **1997**, *386*, 377.
(29) Murata, K.; Kaneko, K.; Kanoh, H.; Kasuya, D.; Takahashi, K.; Kokai, F.; Yudasaka, M.; Iijima, S. *J. Phys. Chem. B* **2002**, *106*, 11132.
(30) Murata, K.; Kaneko, K.; Steele, W. A.; Kokai, F.; Takahashi, K.; Kasuya, D.; Hirahara, K.; Yudasaka, M.; Iijima, S. *J. Phys. Chem. B* **2001**, *105*, 10210.
(31) Shiraishi, M.; Takenobu, T.; Ata, M. *Chem. Phys. Lett.* **2002**, *367*, 633.
(32) Shiraishi, M.; Ata, M. *J. Nanosci. Nanotechnol.* **2002**, *2*, 463.
(33) Ren, S.-L.; Wang, K.-A.; Zhou, P.; Wang, Y.; Rao, A. M.; Meier, M. S.; Selegue, J. P.; Eklund, P. C. *Appl. Phys. Lett.* **1992**, *61*, 124.
(34) Compagnon, I.; Antoine, R.; Broyer, M.; Dugourd, P.; Lerme, J.; Rayane, D. *Phys. Rev. A* **2001**, *64*, 025201.
(35) Goedde, B.; Waiblinger, M.; Jakes, P.; Weiden, N.; Dinse, K.-P.; Weidinger, A. *Chem. Phys. Lett.* **2001**, *334*, 12.
(36) Lebedkin, S.; Ballenweg, S.; Gross, J.; Taylor, R.; Krätschmer, W. *Tetrahedron Lett.* **1995**, *36*, 4971.
(37) Lebedkin, S.; Gromov, A.; Giesa, S.; Gleiter, R.; Renker, B.; Rietschel, H.; Krätschmer, W. *Chem. Phys. Lett.* **1998**, *285*, 210.
(38) Solodovnikov, P. S.; Tumanskii, B. L.; Bashilov, V. V.; Sokolov, V. I.; Lebedkin, S. F.; Krätschmer, W. *Chem. Phys. Lett.* **1999**, *303*, 387.
(39) Yamauchi, S.; Funayama, T.; Ohba, Y.; Paul, P.; Reed, C. A.; Fujiwara, K.; Komatsu, K. *Chem. Phys. Lett.* **2002**, *363*, 199.
(40) Fujitsuka, M.; Ito, O.; Dragoe, N.; Ito, S.; Shimotani, H.; Takagi, H.; Kitazawa, K. *J. Phys. Chem. B* **2002**, *106*, 8562.
(41) Shimotani, H.; Dragoe, N.; Kitazawa, K. *J. Phys. Chem. A* **2001**, *105*, 4980.
(42) Dragoe, N.; Shimotani, H.; Wang, J.; Iwaya, M.; de Bettencourt-Dias, A.; Balch, A. L.; Kitazawa, K. *J. Am. Chem. Soc.* **2001**, *123*, 1294.
(43) Csanyi, G.; Arias, T. A. *Chem. Phys. Lett.* **2002**, *360*, 552.
(44) Kuzmany, H.; Plank, W.; Winter, J.; Dubay, O.; Tagmatarchis, N.; Prassides, K. *Phys. Rev. B* **1999**, *60*, 1005.
(45) Kim, K. C.; Hauke, F.; Hirsch, A.; Boyd, P. D. W.; Carter, E.; Armstrong, R. S.; Lay, P. A.; Reed, C. A. *J. Am. Chem. Soc.* **2003**, *125*, 4024.